High-Resolution Patterned Biobased Thin Films via Self-Assembled Carbohydrate Block Copolymers and Nanocellulose

Marie Gestranius, Issei Otsuka, Sami Halila, Daniel Hermida-merino, Eduardo Solano, Redouane Borsali, Tekla Tammelin

ADVANCED MATERIALS INTERFACES
www.advmatinterfaces.de

High-Resolution Patterned Biobased Thin Films via Self-Assembled Carbohydrate Block Copolymers and Nanocellulose

Marie Gestranius, Issei Otsuka, Sami Halila, Daniel Hermida-Merino, Eduardo Solano, Redouane Borsali, and Tekla Tammelin**

The exploitation of the effortless self-assembly behavior of biomass-based bricks can be seen as a promising route toward the innovative architectures. Here, a straightforward approach is presented where carbohydrate-based diblock copolymer, polystyrene-*block*-maltoheptaose (PS-*b*-MH), is organized either on a rigid ultrathin film or on a flexible self-standing film of wood-derived cellulose nanofibrils (CNFs). During solvent annealing PS-*b*-MH deposited on relatively rough CNF film undergoes spontaneous rearrangement into high-resolution patterns with a diblock domain spacing of 10–15 nm. The ideal conditions the self-assembly require weak interactions between block copolymer and the substrate to increase the chain mobility and enable rearrangements. This is exactly how the system behaves. Adsorption studies of PS-*b*-MH on CNF surfaces reveal weak interactions, and the formed PS-*b*-MH layer is soft and mobile. Even the appearance of more challenging vertical orientation formed on smooth CNF substrates is tentatively evidenced by grazing-incidence small-angle X-ray scattering and atomic force microscope indicating favorable surface interactions between CNF and PS-*b*-MH.

1. Introduction

All carbohydrates including nanocellulosic materials are abundant and a renewable resource that is currently attracting much interest since they can convincingly be used as biocompatible, hydrophilic and bioactive elementary building blocks.[1–3] Nanoscale level self-assembly of carbohydrate-based materials such as cellulose nanofibrils (CNF) and amphiphilic glycopolymers constitute an elegant bottom up approach that will allow the introduction of eco-friendly manufacturing processes. This will unprecedentedly enable the fabrication of continuous high-resolution patterned structures with green, simple and upscalable processes, which can be utilized in next generation devices such as biobased optical structures and nanotemplated membranes.[4,5]

Amphiphilic glycopolymers or more specifically block copolymers (BCPs) are a unique class of polymers, consisting of chemically distinct homopolymers chains that are linked covalently and able to self-assemble into periodic and ordered microdomains at the nanoscale level. In thin films, arrays of BCP microdomains with long-range order can serve as ideal templates or scaffolds for patterning nanoscale functional materials surpassing the size limit of conventional photolithography. Utilizing microphase separation of BCPs as a method for fabricating predictable periodic structures controlled with molecular level precision (≈10–100 nm) has garnered significant attention because of its capacity for generating a high density of microdomains useful in nanotechnology-related applications including nanolithography, nanotemplating, nanoporous membranes, and ultrahigh-density storage media.[6] In the last decade, in Borsali's group, has emerged a new class of BCP associating carbohydrates that is considered as highly incompatible biosourced BCPs allowing their self-assembly on smooth silicon surfaces into well-ordered sub-10 nm scale domains in thin-films.[7–14] To date, the self-assembled nanopattern structures have been constructed mostly on highly smooth and rigid substrates such as silicon and mica. For the next-generation of electronic devices, researchers are currently developing materials that generalize self-assembly BCPs in the field of flexible electronic for their potential use in, e.g., paper-like displays,

M. Gestranius, Prof. T. Tammelin
VTT Technical Research Centre of Finland Ltd.
P.O. Box 1000, 02044-VTT, Finland
E-mail: tekla.tammelin@vtt.fi
Dr. I. Otsuka, Dr. S. Halila, Prof. R. Borsali
Univ. Grenobles Alpes
CNRS
CERMAV
CNRS
CERMAV
38000 Grenoble, France
E-mail: borsali@cermav.cnrs.fr
Dr. D. Hermida-Merino
Netherlands Organization for Scientific Research
DUBBLE beamline at the ESRF
71 Avenue des Martyrs, CS40220, 38043 Grenoble, France
Dr. E. Solano
NCD-SWEET Beamline
ALBA Synchrotron Light Source
08290 Cerdanyola del Vallès, Spain
The ORCID identification number(s) for the author(s) of this article can be found under https://doi.org/10.1002/admi.201901737.

DOI: 10.1002/admi.201901737

plastic radio frequency identification tags and bioimplantable devices.[15–18]

CNFs isolated from plant cell wall can be considered as highly competitive material alternatives not only due to their renewable and green status but also due to their tensile properties coupled with the high inherent tendency to form film structures via the strong interactions between the numerous hydroxyl groups located on the fibril surface.[19–23] Furthermore, amphiphilicity and high hygroscopicity distinguish CNFs from many other nanomaterials that are comparable in terms of high surface areas and strength. Indeed, the strong film formation ability enables numerous opportunities in modern material science and nanotechnology ranging application areas from flat panel displays to water purification membranes, diagnostics and biocatalytic templates.[24–28]

In this context, to further develop the construction of truly nano-organized structures based on carbohydrate sources, the ultimate challenge lies in polydispersity and structural complexity of the plant-derived materials. The inhomogeneity of the cellulose nanofibrils with respect to the size distribution and chemical composition easily leads to surface structures with moderate roughness, which may interfere the formation of the true nanoscaled alignment and order. Furthermore, the methods to fabricate high-resolution nano-organized assembled structures in a controllable and upscalable manner, which facilitate the large-scale production, are very limited. This definitely brings challenges when considering the exploitation of such structures as plant-based flexible substrates for next generation green material concepts in the aforementioned application fields.

Here we report the fabrication of high-resolution nano-organized films by self-assembling carbohydrate-based block copolymers on wood-derived nanocellulose substrates. In order to evaluate the influence of the substrate surface roughness on the alignment of the self-assembled glycopolymer pattern, both rigid and flexible supports were utilized. Polystyrene-*block*-maltoheptaose (PS-*b*-MH) thin film layers were deposited on pure silicon wafers (reference system), on CNF coated silicon wafers and directly on flexible, self-standing CNF films. After the simple solvent vapor annealing step carried out with a mixture of tetrahydrofuran (THF) and water, the formed patterns and the interdomain spacings were analyzed with high resolution imaging techniques (transmission electron microscopy (TEM) and atomic force microscope (AFM)) as well as grazing-incidence small-angle X-ray scattering (GISAXS). Furthermore, the strength of the interactions between block copolymer and cellulose nanofibrils was elaborated by the adsorption experiments using quartz crystal microbalance with dissipation monitoring (QCM-D).

2. Results and Discussion

To demonstrate the feasibility of the concept exploiting the naturally sourced materials, we have selected to construct nanostructures from cellulose nanofibrils, which are either mechanically or mechano-chemically disintegrated from wood pulp fibers. Both utilized CNF grades possess a high film forming tendency, and depending on the size distribution and the overall dimensions of the individual fibrils, the films appear as translucent or fully transparent with the submicron surface roughness levels (**Figure 1**a,b).

The sugar-based block copolymer used in this work ($PS_{3.8k}$-*b*-$MH_{1.2k}$) is composed of maltoheptaose (M_n = 1.153 kg mol^{-1}) that is a size-homogeneous linear heptasaccharide, covalently "clicked" to a narrow polydisperse polystyrene (M_n = 3.8 kg mol^{-1}). The synthesis and detailed characterization of the BCP was described in our previous report.[29] Recently, we have reported a variety of carbohydrate-based "hybrid" block copolymer systems and their self-assembly.[7–11,30,31] These natural/synthetic hybrid block copolymers have higher Flory–Huggins interaction parameters (χ) than current coil–coil or flexible–flexible BCPs made from petroleum because of the high hydrophilicity and the rigid rod-like structures of the carbohydrate blocks. Such a specific character of the carbohydrate-based block copolymers allows sub-10 nm scale self-organized patternings (sphere, cylinder, and lamellae) formed on smooth silicon wafer surfaces, see also Figure 1c.

The approach to construct nanostructured architectures involving nanocellulose and PS-*b*-MH is simple and the processing steps include well known unit operations found in conventional film manufacturing and electronics industry: cast coating, spin coating and annealing. The rigid films based on cellulose nanofibrils on hard substrates were prepared by spin coating of the aqueous dispersion of CNF on silicon substrate. This technique generates smooth and ultrathin films of CNF with the thickness of only tens of nanometers and the roughness is dictated only by the size of the individual fibrils, see also the height scans of the AFM images in Figure 1b. The root mean square (RMS) roughness determined from 5 μm × 5 μm AFM topography image is ≈6 nm for surfaces prepared using uniform and nanosized 2,2,6,6-tetramethyl-1-piperidinyloxy radical (TEMPO) CNF whereas the substrates from larger fibrils produced only by mechanical disintegration give the roughness value of ≈65 nm. These values are well in accordance with previously reported values.[33] For comparison, RMS roughness for pure SiO_2 surface is ≈2 nm (see Figure S1 in the Supporting Information). Similar ultrathin films of CNF have routinely been utilized as substrates in surface sensitive methods for, e.g., polyelectrolyte adsorption and humidity sorption investigations.[32,33] Furthermore, perfectly similar TEMPO CNF ultrathin film have been utilized also in this work to elaborate the block copolymer interactions with CNF using QCM-D.

The manufacturing of the flexible and self-standing CNF films is based on the solvent casting (cast-coating) of the aqueous CNF suspension on a supporting substrate. Adhesion and spreading of the CNF suspension is controlled during drying, and after the evaporation of water, the CNF film is separated from the substrate as a self-standing structure. Such flexible and self-standing structure generates roughness with different length scales resulting in higher variations. Macroscale RMS roughness measured using optical profilometer with 500 μm × 500 μm scan area gives the value of ≈350 nm for TEMPO CNF films and ≈1200 nm for mechanically disintegrated CNF films (see Figure S2 in the Supporting Information). Note that roughness of this length scale cannot be measured for ultrathin films of CNF because their thickness is in

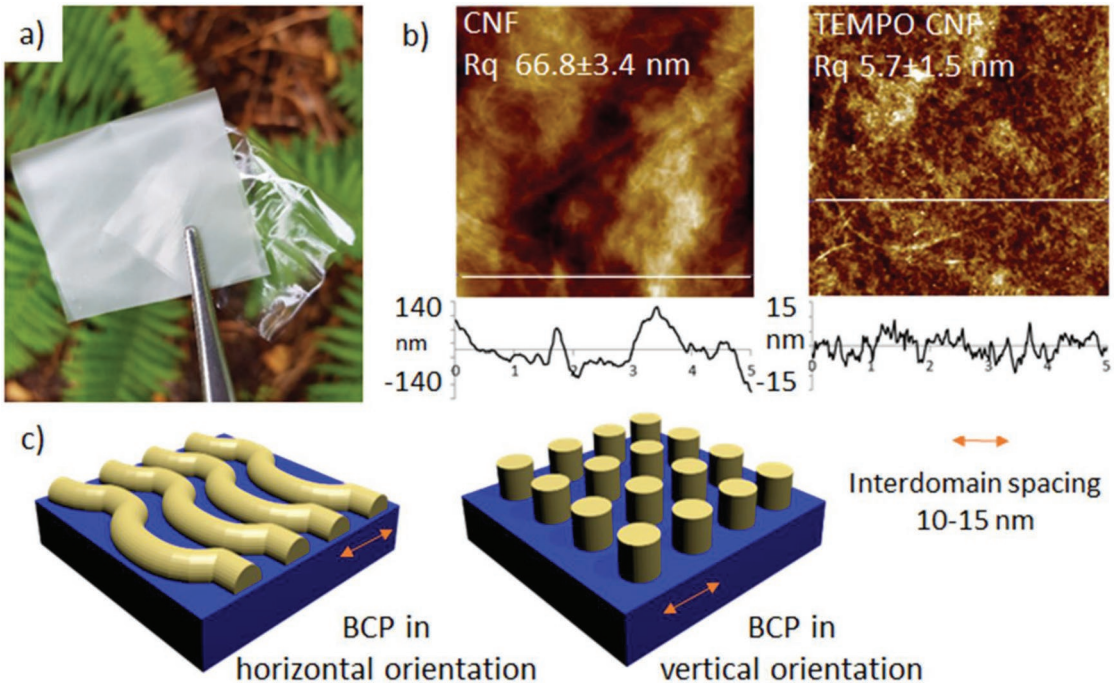

Figure 1. a) Photograph of the flexible and self-standing films constructed using mechanically disintegrated cellulose nanofibrils (translucent CNF film) and TEMPO-oxidized cellulose nanofibrils (transparent TEMPO CNF film). b) 5 µm × 5 µm AFM topography images (left) of mechanically disintegrated CNF and TEMPO-oxidized CNF surfaces indicating the dimensions and the size distribution of the individual fibrils with the corresponding root-mean-square (RMS) roughness values (R_q). Height scans are indicated as white lines in the AFM images. c) Schematic structures of the horizontal (left) and vertical patterns (right) generated via solvent vapor annealing of the deposited polystyrene-*block*-maltoheptaose (PS-*b*-MH) thin films using different water/THF ratios.

real nanometer level. Therefore, ultrathin films can be considered significantly smoother featuring only nanometer level variations whereas than self-standing CNF films display also a macroscale roughness profile.

2.1. Interactions between Block Copolymer and Nanocellulose

First, our aim was to investigate the nature of the interactions between PS-*b*-MH block copolymer and cellulose nanofibrils. In this context, PS-*b*-MH was allowed to adsorb from different water:THF ratios on the TEMPO CNF fibrils. The water:THF ratios of block copolymer dispersions for adsorption experiments were selected based on the stability behavior of the systems. Dispersion stability was analyzed using turbidity profiling as a function of time. A full set of light transmission profiles scanned from dispersions presented in **Figure 2** are shown in the Supporting Information (Figures S3 and S4, Supporting Information). PS-*b*-MH dispersions with a water to THF ratio smaller than 2:4 were transparent, indicating that polymer is fully dissolved and the solvent can be considered as good solvent for the polymer in question. With larger water to THF ratios, the dispersions appear turbid exhibiting the shift from good solvent system toward poor solvent system. PS-*b*-MH starts to form micelles with a particle size varying within of 500–1500 nm (see Table S1 in the Supporting Information). Based on the light scattering data and turbidity profiling, all of the dispersions showed high stability without any tendency to agglomerate or sedimentate. Therefore, for further investigations three different systems were selected: fully soluble block copolymer in good solvent (1:4), boundary conditions where the shift toward poor solvent is expected to take place (2:4, i.e., 1:2) and a system that clearly represents poor solvent system (3:4). The adsorption experiments were carried out using QCM-D with TEMPO CNF ultrathin films, which were deposited on a silica, coated QCM-D sensor surfaces.[33]

As shown in Figure 2, the attraction between the deposited TEMPO CNF layer and the PS-*b*-MH is the most favorable in the water:THF mixture containing larger fraction of water (water:THF ≈3:4) where the highest adsorbed amount of block copolymer on cellulosic surface can be detected. The formed block copolymer layer is relatively soft and mobile seen as significantly higher change in dissipation compared to the adsorption conditions taking place in other water:THF mixtures (1:4 and 1:2). Rinsing with the solvent mixture results in the block copolymer desorption suggesting that the formed layer is rather weakly bound on the CNF surface. Weak interactions with the surface favor the self-assembly to take place allowing block chain mobility needed for their spontaneous rearrangement. The focal driving force for the attractive interactions seems to be related to the solubility of the block copolymer, i.e., polymer adsorbs when polymer–surface and polymer–polymer contacts dominate over the polymer–solvent contacts although adsorption is detected also when the polymer can be considered as fully soluble in water/THF mixtures with high content of THF (water:THF ratios of 1:4 and 1:2).[10] Thus, attractive

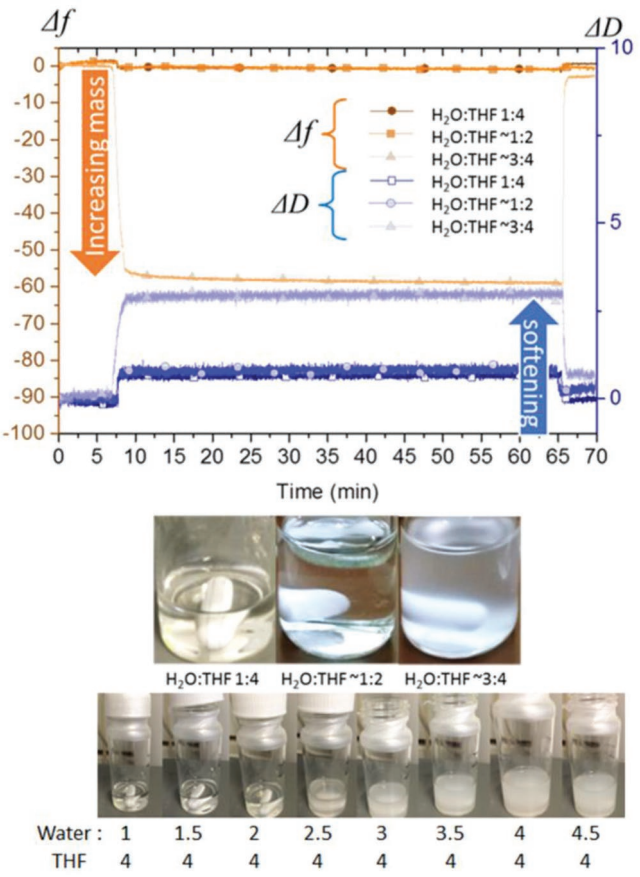

Figure 2. QCM-D data for the adsorption of PS-*b*-MH block copolymer on the TEMPO-oxidized cellulose nanofibrils from three different water/THF mixtures (1:4, ≈1:2 and ≈3:4). Changes in frequency (Δf, orange curves) as a function of time where the negative change is indicating positive mass change detected on the sensor surface (increasing mass due to the adsorption). Blue curves display the changes in dissipation (ΔD) as a function time, which describes the changes in the viscoelastic properties during the adsorption process. Low change in dissipation ($\Delta D < 1 \times 10^{-6}$) indicates the formation of rigid and strongly bound layer whereas higher dissipation changes predict the formation of soft layer with large amount of solvent incorporated in the structure of the adsorbed BCP film. Bottom line photographs portray the appearance of the block copolymer dispersions dissolved in the different ratios of water and THF. Transparent dispersions show the light transmission of >90% whereas turbid dispersions <5%.

carbohydrate–carbohydrate interactions between maltoheptaose blocks and cellulose chains also seem to exist in our system.

2.2. Formation of Continuous Arrays

Straightforward spin coating and solvent annealing procedures were utilized in order to fabricate block copolymer patterns on nanocellulosic substrates via self-assembly. PS-*b*-MH dissolved in THF was spin coated either on smooth and rigid ultrathin films of nanofibrillated cellulose or on flexible and self-standing CNF films with larger roughness variation. Subsequent to block-copolymer spin-coatings, the self-organization were promoted by solvent vapor annealing using different ratios of water:THF mixture according to a slight modified procedure described in Otsuka et al.[10] For the horizontal orientation a 1:1 w/w ratio of water:THF was used and for vertical orientation the water:THF ratio was 1:15 w/w. These particular mixtures favor the block copolymer rearrangement since THF is a selective solvent for the hydrophobic polystyrene block whereas water is selective for the hydrophilic maltoheptaose block.

As shown in the AFM topography images in **Figure 3** clear horizontal block copolymer domain orientations can be generated on smooth and rigid ultrathin films of CNF (nanofibrils attached on SiO_2 substrate) using the appropriate vapor annealing conditions. The pattern features are comparable to those deposited on the reference silicon substrate. Even the surface of mechanically disintegrated CNF spin coated on rigid silica substrate with wider fibrillar size distribution and higher surface roughness serves as a suitable substrate for PS-*b*-MH to display clear horizontal patterns. These findings comprise a solid basis for the further investigations related to the influence of the roughness on the pattern formation. Figure 3b compares the surface morphology of the different surfaces we have utilized for the nanopattern fabrication. Large variations in 3D surface topography are inevitable when considering both forms of the self-standing films of cellulose nanofibrils (TEMPO CNF and unmodified, mechanically disintegrated CNF). This aspect is further illuminated by the height scans of the corresponding AFM images also depicted in Figure 3b, and by direct roughness analysis conducted with AFM and optical profilometer. The macroscale roughness of both self-standing CNF films is varying within 350–1200 nm depending on the fibril source (see Figure S1 in the Supporting Information). This is a completely different order of magnitude compared to the block copolymer domain size, which is ≈10 nm. Despite of the challenges associated with the moderately high roughness profiles of the CNF films and wide differences in structural unit dimensions, Figure 3b evidently shows that the horizontal pattern features are formed also on the self-standing TEMPO CNF film and mechanically disintegrated CNF film surfaces.

It is known that the surface roughness has influence on the behavior of the block copolymers during annealing. Siviniah et al. found that the surface roughness affects the orientation of a polystyrene acrylate block copolymer, suggesting a critical surface roughness for perpendicular orientation.[34] Furthermore, Kulkarni et al. reported that substrates with high surface fractal dimensions have been found to favor perpendicular orientation of polystyrene and acrylate block copolymers.[35] It is worth to notice that the varying surface roughness in their systems were in the same size range as the ones of this study. On the contrary, other studies suggest that a surface roughness over 5 Angstrom would interfere with the formation of nanoscaled lamella.[36] Orienting BCPs on prepatterned surfaces is one route to manipulate the formations of the patterns and aligning horizontal patterns. Horizontal patterns may form straight parallel lines, either parallel or perpendicular to prepatterned surfaces such as channels and arrays of physical or chemical lines made by lithography.[14,18,37–40] The CNF substrates in this study have a pronounced surface roughness, with a completely random orientation, which certainly affects the formation of BCP patterns. However, all BCP systems are case specific, with varying chemistry and polarity of the BCP and annealing conditions, and cannot easily be used to predict the outcome of our study.

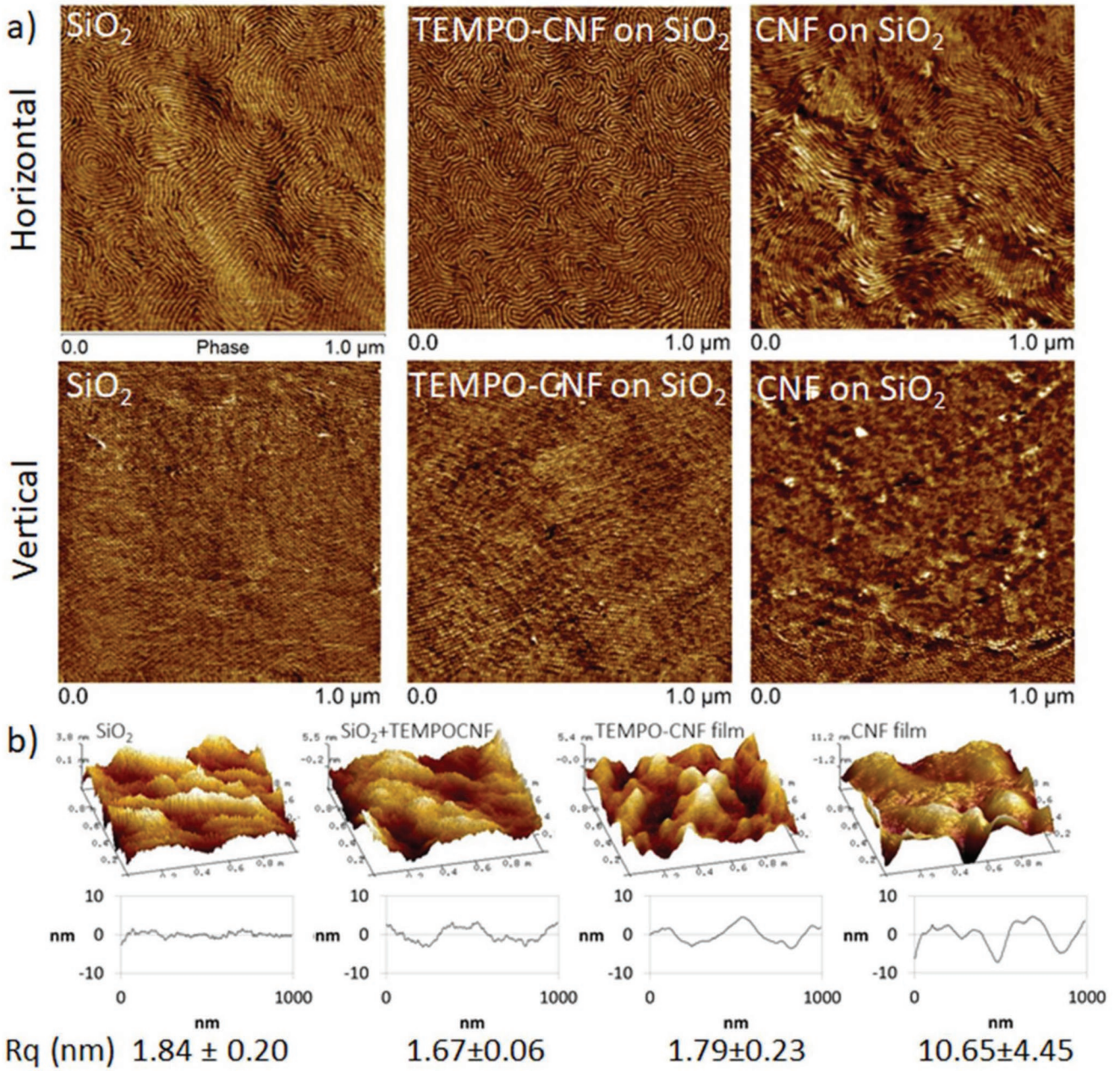

Figure 3. a) 1 µm × 1 µm AFM topography images of the horizontally oriented (top line) and vertically oriented (bottom line) block copolymer patterns on rigid reference silicon supports and the same with TEMPO CNF and mechanically disintegrated CNF thin films spin coated on the silicon substrate. b) 3D AFM topography images with the height scans and corresponding RMS roughness values (R_q) showing how the horizontal patterns are following the structural details of the underlying substrates with increasing surface roughness. Substrates from left to right are the smooth and rigid silicon reference, TEMPO CNF spin coated on the silicon substrate, self-standing and flexible film from TEMPO CNF as well as self-standing, flexible film from mechanically disintegrated CNF.

A remarkable feature is illustrated in the 3D AFM image in **Figure 4**. Horizontal patterns indeed seem follow the valleys and hills of the moderately rough CNF film. In agreement with other studies where the BCPs have been oriented on prepatterned surfaces, the pattern seem to orientate themselves in the direction of the substrate.[37–39]

This is an interesting finding, which currently not have been confirmed by any other means than visual observations. Random orientation of the CNF substrates probably affects the orientation of the BCP but given the complexity of the whole sample matrix, it is challenging to quantify the directions of the pattern in relation to the roughness of the CNF substrate. The AFM phase contrast images (Figure 4) shows clear patterned structure also on the self-standing transparent TEMPO CNF film. In addition, the cross-sectional TEM image reveals the details of the self-assembled block-copolymer layer formed up on the self-standing CNF film. Areas with horizontal orientation are clearly detectable at two different locations in the TEM

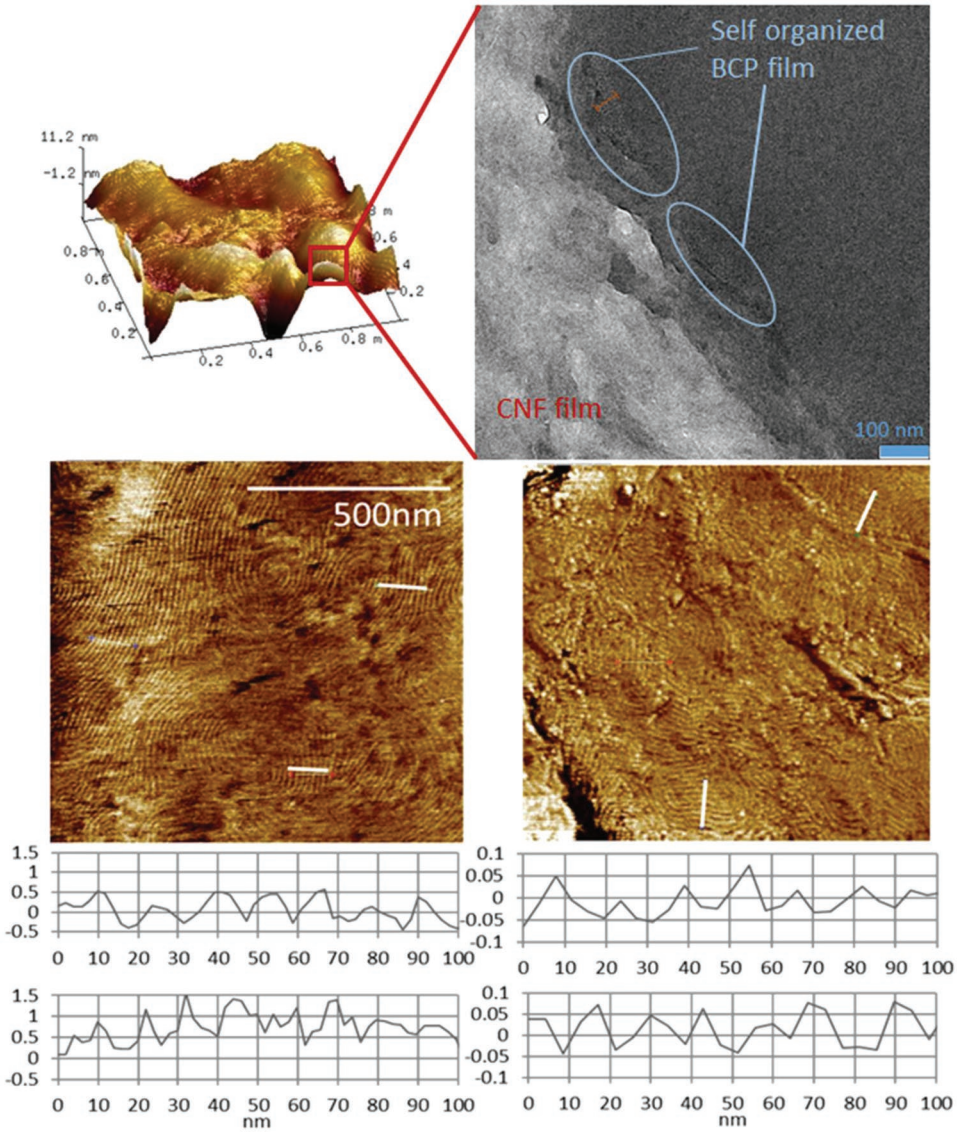

Figure 4. Horizontal orientation of block copolymer (BCP) on a freestanding CNF film can be observed in the AFM 3D map of a sample and in the cross sectional TEM image the structure. Red line in TEM image roughly defines the BCP layer thickness of ≈50 nm. AFM phase contrast images of self-assembled patterns with the white lines indicating the length of 100 nm to be used for the assessment of the pattern block distances. Corresponding pattern profiles are shown underneath the AFM images and 1 μm × 1 μm images of horizontal patterns formed on the flexible and self-standing films constructed using TEMPO-oxidized cellulose nanofibrils (transparent TEMPO CNF film, left) and mechanically disintegrated cellulose nanofibrils (translucent CNF film, right).

images in Figure 4, i.e., dot-patterned images observed in the circles represent that the cylinders of the BCPs oriented from back side to front side (or vice versa) of the image, which indicates the cylinders orient parallel to the BCP film surface. A rough thickness estimation from TEM image yields thickness of ≈50 nm for self-organized BCP layer. An accurate thickness analysis performed by analyzing areal mass changes before and after spin coating of BCP on nanocellulose using QCM-D gives a BCP layer thickness of 33 ± 1.2 nm (see details in Figure S5 in the Supporting Information).

Vertical orientation of PS-*b*-MH is more demanding to achieve, and requires similar surface energies of the substrate, the annealing vapor and both polymer components of the block copolymer. By fine-tuning the water:THF ratio of the annealing vapor, vertical patterns can be formed on SiO_2 substrates.[10] Vertical patterns were observed on CNF and TEMPO CNF on solid support, and AFM image analysis revealed dot-patterned surfaces indicating vertical orientation. Vertical orientation on self-standing CNF and TEMPO CNF films were not found. Regardless of the water/THF ratio, only horizontal patterns were formed on the self-standing films. This could be due to the larger thickness of self-standing films; adsorbing larger amounts of water, creating an environment with higher water content close the film surface, which does not favor vertical orientation. The thickness of the applied BCP layer is probably also decreased and less uniform due to penetration into the

CNF film, which is unfavorable for self-assembly. The high surface roughness of the CNF film in comparison to the domain size of the BCP cylinders might also have a negative effect on the ability to form vertical patterns.

2.3. The Assessment of Interdomain Spacings

The interdomain spacings of the horizontally assembled PS-*b*-MH on CNF films was analyzed with high resolution imaging technique, AFM. AFM phase contrast imaging seems to generate the images of the highest precision for domain spacing evaluation, see Figure 4. As approximated in Figure 4, circa eight peaks fall within the distance of 100 nm resulting in a peak to peak distance of the individual domains of ≈12.5 nm even for CNF film with higher surface roughness. The AFM tip convolution is limiting more exact image analysis; nevertheless, the AFM image analysis indicates the order of magnitude. Grazing-incidence small-angle X-ray scattering of the BCP thin films on CNF solid supports were measured using synchrotron light source to prove the nanostructure order over a large sample volume and thus, with larger statistically data over AFM. **Figure 5** depicts the GISAXS patterns of both, the horizontal (Figure 5a) and vertical (Figure 5b) aligned PS-*b*-MH on CNF films. Both recorded GISAXS patterns showed a main scattering peak ca. $q_y = 0.5$ nm^{-1}. In order to assess the maximum q_y position of the main peak (q^*), horizontal cuts along q_y at the q_z maximum of the main lobe were done. Figure 5c depicts the horizontal q_y cuts of both samples, clearly showing the position of the main peak and the presence of a low intensity second order peak, which is hardly visible on the recorded image. In fact, the sample containing vertically [horizontally] aligned cylinders presented a main scattering peak at $q_{y,1}^* = 0.509$ [$q_{y,2}^* = 0.579$] nm^{-1}, with a second order signal at $2q_{y,1}^*$ [$\sqrt{3}q_{y,2}^*$]. The $\sqrt{3}q_{y,2}$ relation between the first and second order signal of the sample with BCPs aligned with the substrate plane was consistent with a hexagonal packing, while the cylinders aligned vertically with relation $2q_{y,1}^*$ indicated a pseudocubic order of the BCPs. Moreover, the center-to-center distance between the packing units can be determined by the main peak q_y^* position. Therefore, for a hexagonal lattice, the q_y^* position can be converted to real space distance by the formula: $D = 4\pi/(\sqrt{3}q_y^*)$, while the cubic lattice conversion is given by $D = 2\pi/q_y^*$. As result, the horizontal aligned cylinders presented a distance between the centers of the cylinders of 12.5 nm, while for the vertically aligned cylinders was 12. 3 nm, results that are in line with the AFM data. Ring-like and hexagonal patterns observed in the fast Fourier transform (FFT)

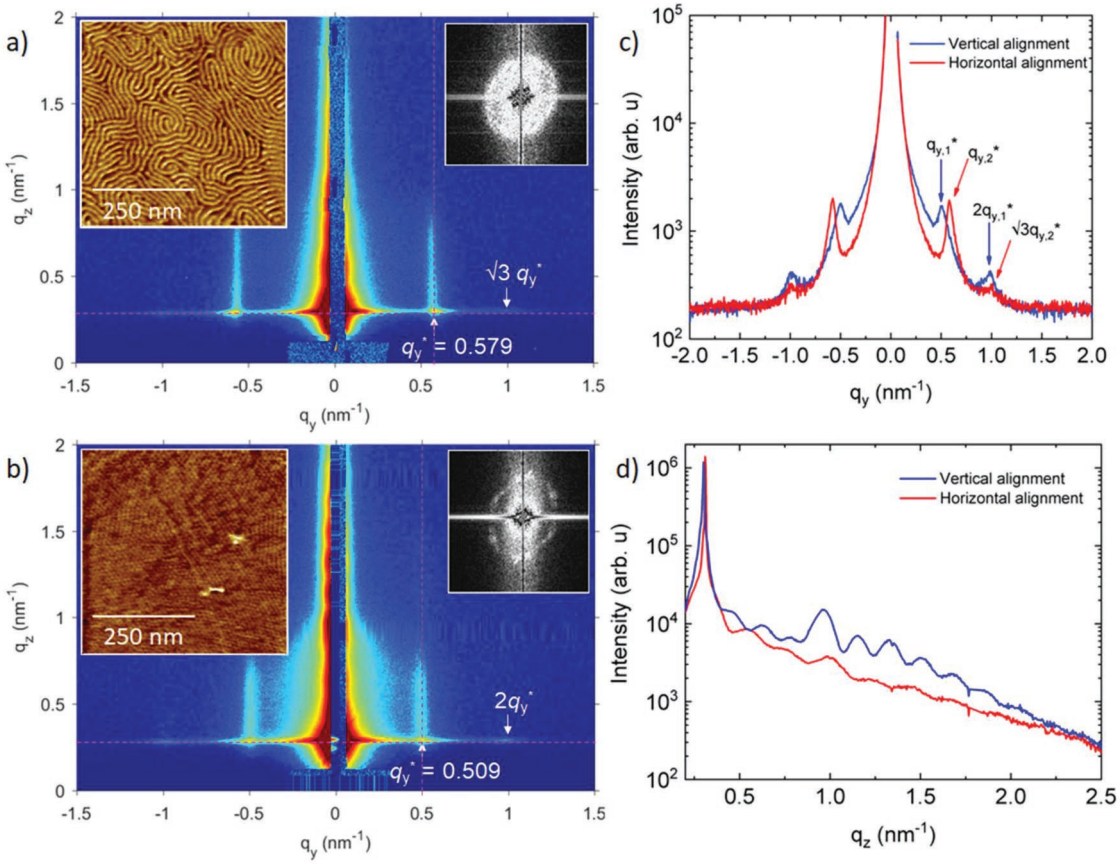

Figure 5. GISAXS 2D scattering patterns recorded at X-ray incident angle of 0.13° of a) PS-*b*-MH on CNF films on solid support annealed to horizontal orientation and b) PS-*b*-MH on CNF films on solid support annealed to vertical orientation. The AFM height image insets show the respective orientations on TEMPO CNF films on solid support. The black and white insets displays the fast Fourier transformation of the corresponding AFM images. c) Horizontal q_y cuts at the q_z maximum of the main lobe peak position. d) Vertical q_z cuts at $q_y = 0.1$ nm^{-1} for both recorded GISAXS patterns.

images from the AFM images shown as insets in Figure 5a,b suggest the random distribution of horizontal cylinders and the hexagonally close-packed vertical cylinder/cubic lattices on the surface of the films. Complementarily, vertical q_z cuts at low q values (i.e., $q_y = 0.1$ nm^{-1}) were done to qualitative obtain out-of-plane information. Figure 5d depicts the vertical cuts of both investigated samples, where the vertical aligned cylinders presented higher number contributions when compared with the sample containing the horizontal cylinders. This could be due not only to the total thickness of the thin film layer and the BCP ordering, but also to the contribution of the surface roughness. Further investigations are required to discern and totally understand the contributions of the nanostructured layer, surface roughness and BCPs ordering on the vertical q_z cut. The qualitative analysis of the 2D GISAXS images could give information about the formation and arrangement of the BCP cylinders: the presence of a main q_y scattering lobe for the horizontal aligned cylinders together with the higher number of contributions along q_z for the vertically aligned BCPs suggested that first, ellipsoidal micelles of the BCPs were formed for later forming packed cylinders as the solvent is evaporated. The orientation of these initial micelles would determine the final BCP cylinder orientation.[41,42] In fact, due to the high χ parameter of the two polymer chains forming the structure, the hydrophilic block would be expected to face the solvent and hence, would form a hydrophobic micelle core.

3. Conclusions

High-resolution self-assembled patterns of carbohydrate-based block copolymer with interdomain spacings of 10–15 nm can be fabricated nanocellulose substrates. It is highly encouraging that these patterns are formed even on rough, flexible and self-standing nanocellulose films. PS-*b*-MH deposited on relatively rough CNF films spontaneously self-assemble forming horizontal periodic structures. The horizontally oriented patterns seem to align on the surface of the nanocellulose film tracing its topographical features. Even the appearance of more challenging vertical orientation formed on nanocellulose was evidenced by GISAXS and AFM indicating the compatible surface energetics between nanocellulose and PS-*b*-MH. Generally, it was observed that the interactions between PS-*b*-MH and nanocellulose were weak, and the formed PS-*b*-MH layer was soft and mobile, indicating a favorable environment for self-assembly to take place. The tentative appearance of vertical patterns is an inspiring finding, and warrants further research with the potential in nanotechnology-related applications, e.g., as nanotemplated membranes and biosensors.

4. Experimental Section

Preparation of Cellulose Nanofibrils: Two different grades of CNF were utilized, namely, mechanically disintegrated cellulose nanofibrils and TEMPO oxidized cellulose nanofibrils (TEMPO CNF).[43,44] Mechanically disintegrated CNFs were prepared from never dried bleached birch kraft pulp obtained from the Finnish pulp mill. The pulp was first soaked at 1.7% consistency and dispersed using a high shear Diaf dissolver (Minibatch Type20) for 10 min at 700 rpm. The pulp suspension was pre-refined in a Masuko grinder (Supermasscolloider MKZA10-15J, Masuko Sangyo Co., Japan) at 1500 rpm and fluidized with six passes through a Microfluidizer (Microfluidics M-7115-30 Microfluidicis Corp.). The mechanical disintegration resulted in a material of a viscous and translucent gel of cellulose nanofibrils (light transmittance of 58% at 800 nm by UV–vis spectroscopy) with a final solid content of ≈1.6%.

TEMPO-oxidized cellulose nanofibrils (TEMPO CNF) were produced from bleached softwood kraft pulp obtained from the Finnish pulp mill. Prior to the fibrillation, the pulp was TEMPO-oxidized according to a protocol described by Saito et al.[43] The degree of oxidation per anhydroglucose unit of cellulose was at the level of 1.2 mmol g^{-1} determined by conductometric titration of pulp (SCAN-CM 65:02, 2002). The washed TEMPO-oxidized chemical pulp suspension was fluidized with two passes through the Microfluidizer. The mechanical disintegration resulted in a viscous and transparent gel (light transmittance of 74.3% at 800 nm by UV–vis spectroscopy) with a final solid content of ≈1.2%.

Fabrication of Smooth and Rigid Ultrathin CNF Films on Solid SiO_2 Support: SiO_2 wafers (supplied by Okmetic, Espoo, Finland) were cleaned by immersing in 10% NaOH for 10 min, and then carefully rinsed with Milli-Q water. The cleaned wafers were dried with nitrogen gas (N_2) and stored in ethanol until further use.

Supported ultrathin films of CNF and TEMPO CNF were prepared with a protocols described by Eronen et al. and further modified by Hakalahti et al. with spin coater (WS-400BZ-6NPP/Lite, Laurell, North Wales, PA, USA).[33,45] Prior to CNF or TEMPO CNF deposition, a layer of anchoring polymer (polyethylene imine (PEI)) was adsorbed onto the silicon substrate by immersing the substrate in 1 mg mL^{-1} PEI solution for 30 min. The excess of PEI was rinsed away with large amounts of Milli-Q water, followed by nitrogen gas drying and oven drying at 80 °C for 10 min. Prior to the spin coating of nanocellulose dispersions the silica surface was wetted by spin coating a 100 µL of Milli-Q water on the wafer at 3000 rpm for 10 s. Then 100 µL of 0.15% CNF or TEMPO CNF dispersions were immediately spin coated at 3000 rpm for 45 s. Finally, the spin coated surfaces were oven dried at 80 °C for 10 min, resulting in evenly covered solid substrates as previously reported by Tenhunen et al. and Hakalahti et al.[33,46]

Fabrication of the Flexible CNF Films: Self-standing films of CNF and TEMPO-CNF were prepared with a patented cast coating method which is described in detail in Mäkelä et al.[4,47] Briefly, the undiluted CNF or TEMPO CNF gels with sorbitol (30 wt% of dry film, Sigma-Aldrich) were mixed together, first with a high shear rotor stator mixer (Ultra Turrax T25, IKAWorks, Wilmington, NC, USA) at ≈15 000 rpm for 1 min and later with a speedmixer (SpeedMixer DAC 1100.1 VAC-P, Hauschild Engineering, Germany) at 1600 rpm for 10 min. Due to very brittle character of the TEMPO CNF films, polyvinyl alcohol (PVA, Mowiol 56–98, M_w 195 000, 10 wt% of dry film from Sigma-Aldrich) was used to enhance the strength properties. Nanocellulose gel was cast with a 2 mm manually operated slot coater onto a plasma treated low density polypropylene (LDPP) film and air-dried at ambient conditions for 24 h. The formed CNF or TEMPO CNF films were separated from the plastic supports and for the further treatments, pieces of films were cut to the approximate size of 1.0 cm × 1.5 cm. The film pieces were carefully attached on glass supports using Kapton tape.

The thickness of the self-standing CNF and self-standing TEMPO CNF films was measured using a Lorentzen and Wettre L&W micrometer 51 measurement device (Lorentzen and Wettre, Sweden). The reported thickness values are average of three measurements being 21.3 ± 2.1 and 21.0 ± 1.7 µm for CNF films and TEMPO CNF films, respectively.

Macroscale roughness of self-standing CNF and TEMPO CNF were measured white light interferometry using a Veeco Wyko NT9100 optical profilometer (Veeco Instruments Inc, Plainview, United States).[48] RMS roughness values (R_q) are derived from 500 µm × 500 µm representative area of the films. Note that the R_q values for clean SiO_2 surfaces, and CNF and TEMPO CNF films deposited on solid SiO_2 support were all below 2.0 nm and too smooth for precise characterization with the white light interferometry technique.

Synthesis of the PS-b-Maltoheptaose Glycopolymers: The amphiphilic glycopolymer was obtained according to a modified procedure reported by Aissou et al.[7] A new copper catalytic system as well as an additional step of resin purification allowed the readily synthesis of glycopolymer and the removal of remaining copper catalysts, respectively. Briefly, the ω-azido-terminated polystyrene (1 equiv., 8.1 g, 1.8×10^{-3} mol) was clicked to alkynyl-terminated maltoheptaose (1.2 equiv., 2.7 g, 1.8×10^{-3} mol) in degassed dimethylformamide solution and catalyzed by Cu nanopowder (1.8 equiv., 260 mg, 3.2×10^{-3} mol). The reaction mixture was warmed up to 65 °C and monitored by 1H nuclear magnetic resonance (NMR) of the relevant adjacent azide-bearing methylene protons until total conversion. The crude heterogeneous mixture was passed through a pad of Celite, and the filtrate was stirred several hours in the presence of the Cuprisorb resin. The mixture was finally precipitated in cold MeOH to give a white powder with a yield of 80% (mass = 8 g). The 1H NMR and matrix-assisted laser desorption/ionization analyses are in perfect agreement with those previously reported elsewhere.[13]

Stability and Particle Size of PS-b-MH Dispersions: The light transmission profiles of 0.015 g of PS-*b*-MH dissolved in 15 mL of solutions containing different ratios of Milli-Q water and THF were measured with Turbiscan LAB (Formulaction SA, L'Union, France). Information of the sample stability was obtained by scanning the sample in vertical direction (over the length of the sample cell) over a time interval, with a total measurement time of 10 min, with one scan in the beginning and one at the end of the measurement.[49] One set of measurement data was collected for one hour every 10 min to test the stability of the sample with the highest water content over a longer period of time.

Dynamic light scattering was used to determine the hydrodynamic diameter (particle size) of turbid dispersions block copolymers. Samples of 0.015 g of PS-*b*-MH dissolved in 15 mL solvent containing different ratios of water and THF were analyzed with a Malvern Zetasizer Nano ZS90 (Malvern Panalytical Ltd, United Kingdom) at 30 °C. Based on the data acquired from Nayak et al. the refractive index η_D was roughly estimated to 1.3994 and the viscosity to 0.574 mPa s for samples containing a water to THF ratio of 2.5:4 and for samples with a water to THF larger than 3:4 to 1.3946 and 0.793 mPa s.[50]

Fabrication of the Patterned Structures: A 0.5 wt% solution of polystyrene-*block*-maltoheptaose (PS-*b*-MH) diblock copolymer was prepared by dissolving the polymer in THF followed by stirring overnight at ambient room conditions. 100 µL of the dissolved polymer solution was spin coated on rigid substrates (SiO_2 as reference surface, CNF surfaces and TEMPO CNF surfaces) with the spinning speed of 2000 rpm for 30 s. The spin coating conditions were the same for flexible CNF surfaces (CNF self-standing film and TEMPO CNF self-standing film taped on glass supports), expect for the spinning time of 3 min. The PS-*b*-MH coated CNF surfaces were solvent vapor annealed in 100 mL glass beakers. The samples were placed in solvent resistant holders on the bottom of the beaker. 5 g of premixed water and THF solution was added to a 10 mL beaker, which also was placed inside the 100 mL beaker. The 100 mL beaker was sealed with two layers of Parafilm and a glass Petri dish. The samples were annealed in the vapor generated at different ratios of water and THF for 24 h. For the horizontal orientation, a water/THF ratio of 1:1 w/w was used whereas for the vertical orientation the water/THF ratio was 1:15 w/w ratio.

High-Resolution Microscopical Characterization: The fine structure of the CNF films and block copolymer patterns were analyzed using atomic force microscope (Nanoscope IIIa Multimode scanning probe, Digital Instruments Inc., Santa Barbara, CA, USA) equipped with an E-scanner. Images were taken in tapping mode with silicon cantilevers (HQ-NSC 15-Al BS, Nano And-More GmbH, Germany) with the nominal resonance frequencies of 325 kHz with a tip radius of ≈8 nm. Prior to the imaging, the samples were stored in a desiccator protected from light, for at least 24 h. Images were taken at the resolution of 1×1 µm and at 500×500 nm when the surface roughness of the CNF film did not interfere with the image capturing at the higher resolution. At least three different areas on each sample were analyzed and no image processing except flattening was performed.

Root-mean-square roughness values (R_q) were obtained from AFM images using SPIP software (Image Metrology A/S, Lyngby, Denmark) after flattening of images and applying an ISO 16610 Gaussian 5 mm L-filter.

TEM observations were carried out using a CM200 Philips microscope (Hillsboro, OR) operating at 80 kV. The film sample was embedded in Embed-812 resin, polymerized for 48 h at 60 °C and then cut with an ultramicrotome (UC6 LEICA). The sections are 90 nm thick.

Quartz Crystal Microbalance with Dissipation Monitoring: Thickness analysis and adsorption experiments of PS-*b*-MH on nanocellulose was investigated with the QCM-D Instrument (Q-sense E4, Q-sense, Gothenburg, Sweden). Cellulose nanofibrils were deposited on SiO_2 coated QCM-D sensor surfaces using the same procedure as described above. The SiO_2 coated sensor crystals were AT-cut quartz crystals supplied by Q-sense AB, Gothenburg, Sweden. Via QCM-D in situ studies of mass changes at solid/gas and solid interface can be followed. The interpretation of QCM-D data is described elsewhere in detail.[51–53]

The thicknesses of PS-*b*-MH film deposited on nanocellulose surface was determined by measuring a change in areal mass before and after spin coating of the block copolymer. The piezoelectric sensor crystal oscillates with a resonance frequency that changes when mass change occurs on the sensor surface. The change in areal mass can be calculated using the Sauerbrey equation (Equation (1))[54]

$$\Delta m = -C\frac{\Delta f}{n} \tag{1}$$

where Δm is the change in areal mass, C is a constant that describes the sensitivity of the device to changes in mass, $\Delta f = f - f_0$ is the change in frequency, and n is the overtone number. In this case, $C \approx 0.177$ mg m^{-2} Hz^{-1} and $n = 1, 3, 5, 7, 9, 11, 13$, and $f_0 = 5$ MHz. The areal mass is further converted to thickness using Equation (2), using the theoretical density of PS-*b*-MH = 1190 kg m^{-3}[55]

$$h = \frac{\Delta m_{Sauerbrey}}{\rho_{PS-b-MH}} \tag{2}$$

Adsorption experiments were carried out as follows. Mixtures with different w/w ratios of water and THF (1:2, ≈1:4, ≈3:4) were prepared and allowed to stabilize overnight. 1 mg mL^{-1} PS-*b*-MH solutions were prepared from the water/THF mixture and stirred gently overnight. The water/THF mixtures with the ratios of 1:2 and ≈1:4 appeared as clear solutions (highly soluble polymer solution) whereas the water/THF mixture with the ratio of ≈3:4 appeared slightly turbid indicating the formation of the colloidal, not fully soluble PS-*b*-MH dispersion.

The adsorption of block copolymer on TEMPO CNF surface as well as the desorption subsequent to rinsing were detected by following the changes in frequency (Δf) and dissipation (ΔD) as a function of time for 60 min. Prior to the introduction of the block copolymer into the QCM-D chamber, the TEMPO CNF surfaces were contacted with the corresponding water:THF mixtures for ≈5 min to avoid the bulk effect. Then, ≈1 mL of block copolymer solution dissolved in the same ratio of water and THF was injected into measurement chamber, and the flow was halted for 60 min for the adsorption to take place. After the adsorption, the surface was again rinsed for 5 min with the same water:THF solution. The flow rate used in the adsorption tests was ≈0.2–0.4 mL min^{-1}, and it was manually controlled using a syringe. Each measurement was repeated at least twice.

Grazing-Incidence Small-Angle X-Ray Scattering: Patterns were recorded in BM26B DUBBLE beamline at the European Synchrotron Radiation Facility (ESRF, Grenoble, France).[56,57] A monochromatic X-ray beam of 11.98 keV was set using a Si (111) double crystal monochromator. An incident angle of 0.13° was employed for the GISAXS measurements, ensuring a surface sensitivity configuration. The scattered radiation was recorded using a Pilatus3 S 1M detector (Dectris, Switzerland) located at 2500 mm from the sample, which consists of a pixel array of 1043×981 ($V \times H$) with a pixel size of 0.172×0.172 mm^2. The sample to detector distance, beam center and the reciprocal space calibration were calculated using Silver Behenate as calibrant. GISAXS patterns were calibrated and analyzed using an in-house programmed Matlab

routine. Horizontal q_y and vertical q_z line cuts were done integrating a line cut of 10 pixels in order to enhance the statistics of the signal.

Supporting Information

Supporting Information is available from the Wiley Online Library or from the author.

Acknowledgements

M.G. and I.O. contributed equally to this work. This work was partially supported by the CNRS and the European project "GreeNanoFilms" which has received funding from the European Union Seventh Framework Program (FP7/2007-2013) under grant agreement no. 603519 and Carnot PolyNat Institute (ANR No. 16-CARN-025-01). The work was partially supported by Academy of Finland project CINERGY (ID 300367). The authors acknowledge C. Lancelon-Pin for the cross-sectional TEM observation at CERMAV (ICMG Platform-Grenoble). Katja Pettersson and Suvi Arola (VTT) are acknowledged for assisting AFM imaging. Mari Leino (VTT) is acknowledged for white light interferometry measurements. Anastasia Ivanova (VTT) is acknowledged for assistance with the table of content graphics. The authors would like to thank the DUBBLE team at the ESRF for the assistance during the experiments. This work was a part of the Academy of Finland's Flagship Programme under Project Nos. 318890 and 318891 (Competence Center for Materials Bioeconomy, FinnCERES).

Conflict of Interest

The authors declare no conflict of interest.

Keywords

carbohydrate-based block copolymers, cellulose nanofibrils, green materials, self-assembly, thin films

Received: October 11, 2019
Revised: January 13, 2020
Published online: February 16, 2020

[1] C. Schatz, S. Lecommandoux, *Macromol. Rapid Commun.* **2010**, *31*, 1664.
[2] a) D. Klemm, F. Kramer, S. Moritz, T. Lindström, M. Ankerfors, D. Gray, A. Dorris, *Angew. Chem., Int. Ed.* **2011**, *50*, 5438; b) *Angew. Chem.* **2011**, *123*, 5550.
[3] E. Kontturi, P. Laaksonen, M. B. Linder, Nonappa, A. H. G, O. Rojas, O. Ikkala, *Adv. Mater.* **2018**, *30*, 1703779.
[4] T. Mäkelä, M. Kainlauri, P. Willberg-Keyriläinen, T. Tammelin, U. Forsström, *Microelectron. Eng.* **2016**, *163*, 1.
[5] Y. Miura, H. Seto, M. Shibuya, Y. Hoshino, *Faraday Discuss.* **2019**, *219*, 154.
[6] M. Luo, T. H. Epps III, *Macromolecules* **2013**, *46*, 7567.
[7] K. Aissou, I. Otsuka, C. Rochas, S. Fort, S. Halila, R. Borsali, *Langmuir* **2011**, *27*, 4098.
[8] J. D. Cushen, I. Otsuka, C. M. Bates, S. Halila, S. Fort, C. Rochas, J. A. Easley, E. L. Rausch, A. Thio, R. Borsali, C. G. Willson, C. J. Ellison, *ACS Nano* **2012**, *6*, 3424.
[9] I. Otsuka, T. Isono, C. Rochas, S. Halila, S. Fort, T. Satoh, T. Kakuchi, R. Borsali, *ACS Macro Lett.* **2012**, *1*, 1379.
[10] I. Otsuka, S. Tallegas, Y. Sakai, C. Rochas, S. Halila, S. Fort, A. Bsiesy, T. Baron, R. Borsali, *Nanoscale* **2013**, *5*, 2637.
[11] I. Otsuka, Y. Zhang, T. Isono, C. Rochas, T. Kakuchi, T. Satoh, R. Borsali, *Macromolecules* **2015**, *48*, 1509.
[12] Y. Sakai-Otsuka, S. Zaioncz, I. Otsuka, S. Halila, P. Rannou, R. Borsali, *Macromolecules* **2017**, *50*, 3365.
[13] Y. Liao, W.-C. Chen, R. Borsali, *Adv. Mater.* **2017**, *29*, 1701645.
[14] I. Otsuka, N. Nilsson, D. B. Suyatin, I. Maximov, R. Borsali, *Soft Matter* **2017**, *13*, 7406.
[15] J. A. Rogers, T. Someya, Y. Huang, *Science* **2010**, *327*, 1603.
[16] D. Akinwande, N. Petrone, J. Hone, *Nat. Commun.* **2014**, *5*, 5678.
[17] C.-C. Hung, Y.-C. Chiu, H.-C. Wu, C. Lu, C. Bouilhac, I. Otsuka, S. Halila, R. Borsali, S.-H. Tung, W.-C. Chen, *Adv. Funct. Mater.* **2017**, *27*, 1606161.
[18] H.-C. Kim, C. T. Rettner, L. Sundström, *Nanotechnology* **2008**, *19*, 235301.
[19] Y. C. Hsieh, H. Yano, M. Nogi, S. J. Eichhorn, *Cellulose* **2008**, *15*, 507.
[20] N. Lavoine, I. Desloges, A. Dufresne, J. Bras, *Carbohydr. Polym.* **2012**, *90*, 735.
[21] A. Isogai, T. Saito, H. Fukuzumi, *Nanoscale* **2011**, *3*, 71.
[22] T. Matsunaga, Y. Ikada, *ACS Symp. Ser.* **1980**, *121*, 391.
[23] S. Belbekhouche, J. Bras, G. Siqueira, C. Chappey, L. Lebrun, B. Khelifi, S. Marais, A. Dufresne, *Carbohydr. Polym.* **2011**, *83*, 1740.
[24] M. Nogi, H. Yano, *Appl. Phys. Lett.* **2009**, *94*, 233117.
[25] A. Mautner, K.-Y. Lee, P. Lahtinen, M. Hakalahti, T. Tammelin, K. Li, A. Bismarck, *Chem. Commun.* **2014**, *50*, 5778.
[26] M. Hakalahti, A. Mautner, L.-S. Johansson, T. Hänninen, H. Setälä, E. Kontturi, A. Bismarck, T. Tammelin, *ACS Appl. Mater. Interfaces* **2016**, *8*, 2923.
[27] H. Orelma, I. Filpponen, L.-S. Johansson, M. Österberg, O. Rojas, J. Laine, *Biointerphases* **2012**, *7*, 61.
[28] M. Jämsä, S. Kosourov, V. Rissanen, M. Hakalahti, J. Pere, J. A. Ketoja, T. Tammelin, Y. Allahverdiyeva, *J. Mater. Chem. A* **2018**, *6*, 5825.
[29] Y. Liao, L. J. Goujon, E. Reynaud, S. Halila, A. Gibaud, B. Wei, R. Borsali*Carbohydr. Polym.* **2019**, *212*, 222.
[30] T. Isono, I. Otsuka, Y. Kondo, S. Halila, S. Fort, C. Rochas, T. Satoh, R. Borsali, T. Kakuchi, *Macromolecules* **2013**, *46*, 1461.
[31] T. Isono, I. Otsuka, D. Suemasa, C. Rochas, T. Satoh, R. Borsali, T. Kakuchi, *Macromolecules* **2013**, *46*, 8932.
[32] M. Galván, M. S. Peresin, P. Mocchiutti, N. Granqvist, M. Zanuttini, T. Tammelin, *Cellulose* **2015**, *22*, 2955.
[33] M. Hakalahti, M. Faustini, C. Boissière, E. Kontturi, T. Tammelin, *Biomacromolecules* **2017**, *18*, 2951.
[34] E. Sivaniah, Y. Hayashi, S. Matsubara, S. Kiyono, and T. Hashimoto, K. Fukunaga, E. J. Kramer, T. Mates, *Macromolecules* **2005**, *38*, 1837.
[35] M. M. Kulkarni, K. G. Yager, A. Sharma, A. Karim, *Macromolecules* **2012**, *45*, 4303.
[36] S. Kundu, R. Ganesan, N. Gaur, M. S. M. Saifullah, H. Hussain, H. Yang, C. S. Bhatia, *Sci. Rep.* **2012**, *2*, 617.
[37] R. Ruiz, N. Ruiz, Y. Zhang, R. L. Sandstrom, C. T. Black, *Adv. Mater.* **2007**, *19*, 2157.
[38] S.-M. Park, M. P. Stoykovich, R. Ruiz, Y. Zhang, C. T. Black, P. F. Nealy, *Adv. Mater.* **2007**, *19*, 607.
[39] J. Y. Cheng, J. Pitera, O.-H. Park, M. Flickner, R. Ruiz, C. T. Black, H.-C. Kim, *Appl. Phys. Lett.* **2007**, *91*, 143106.
[40] S. W. Hong, J. Huh, X. Gu, D. H. Lee, W. H. Jo, S. Park, T. Xu, T. P. Russell, *Proc. Natl. Acad. Sci. USA* **2012**, *109*, 1402.
[41] J. J. van Franeker, D. Hermida-Merino, C. Gommes, K. Arapov, J. J. Michels, R. A. J. Janssen, G. Portale, *Adv. Funct. Mater.* **2017**, *27*, 1702516.
[42] G. Fleury, D. Hermida-Merino, D. Jingjin, K. Aissou, A. Bytchkov, G. Portale, *Adv. Funct. Mater.* **2019**, *29*, 1806741.

[43] H. Kangas, P. Lahtinen, A. Sneck, A. M. Saariaho, O. Laitinen, E. Hellen, *Nord. Pulp Pap. Res. J.* **2014**, *29*, 129.
[44] T. Saito, Y. Nishiyama, J.-L. Putaux, M. Vignon, A. Isogai, *Biomacromolecules* **2006**, *7*, 1687.
[45] P. Eronen, J. Laine, J. Ruokolainen, M. Österberg, *J. Colloid Interface Sci.* **2012**, *373*, 84.
[46] T. Tenhunen, M. S. Peresin, P. A. Penttilä, J. Pere, R. Serimaa, T. Tammelin, *React. Funct. Polym.* **2014**, *85*, 157.
[47] T. Tammelin, U. Hippi, A. Salminen, *WO/2013/060934*, **2013**.
[48] M. Andresen, L.-S. Johansson, B. S. Tanem, P. Stenius, *Cellulose* **2006**, *13*, 665.
[49] T. Tenhunen, T. Pöhler, A. Kokko, H. Orelma, M. Schenker, P. Gane, T. Tammelin, *Nanomaterials* **2018**, *8*, 651.
[50] J. N. Nayak, M. I. Aralaguppi, B. V. K. Naidu, T. M. Aminabhavi, *J. Chem. Eng. Data* **2004**, *49*, 468.
[51] M. Rodahl, F. Höök, A. Krozer, P. Brzezinski, B. Kasemo, *Rev. Sci. Instrum.* **1995**, *66*, 3924.
[52] F. Höök, M. Rodahl, P. Brzezinski, B. Kasemo, *Langmuir* **1998**, *14*, 729.
[53] I. Reviakine, D. Johannsmann, R. P. Richter, *Anal. Chem.* **2011**, *83*, 8838.
[54] G. Sauerbrey, *Z. Phys.* **1959**, *155*, 206.
[55] T. Tammelin, R. Abburi, M. Gestranius, C. Laine, M. Österberg, *Soft Matter* **2015**, *11*, 4273.
[56] M. Borsboom, W. Bras, I. Cerjak, D. Detollenaere, D. Glastra van Loon, P. Goedtkindt, M. Konijnenburg, P. Lassing, Y. Levine, B. Munneke, *J. Synchrotron Radiat.* **1998**, *5*, 518.
[57] G. Portale, D. Cavallo, G. C. Alfonso, D. Hermida-Merino, M. van Drongelen, L. Balzano, G. W. M. Peters, J. G. P. Goossens, W. Bras, *J. Appl. Crystallogr.* **2013**, *46*, 1681.